chemosensors

MDPI

Article

Portable Multi-Spectral Sensing Platform and Self-Metering Microfluidic Strips for Quantitative Monitoring of *o*-Phthalaldehyde Disinfectants

Hsien-Yi Hsiao *, Tzong-Jih Cheng, Hung-Yu Chen and Richie L. C. Chen

Department of Biomechatronics Engineering, College of Bio-Resources and Agriculture, National Taiwan University, Taipei 106, Taiwan; tzongjih@ntu.edu.tw (T.-J.C.); d13631001@ntu.edu.tw (H.-Y.C.); rlcchen@ntu.edu.tw (R.L.C.C.)

* Correspondence: f92631001@ntu.edu.tw

Abstract

Routine monitoring of *ortho*-phthalaldehyde (OPA) disinfectants is critical for endoscope reprocessing, yet commercial test strips suffer from subjective visual ambiguity, strict manual timing, and susceptibility to sample matrix dilution. This study proposes a portable multi-spectral colorimetric sensing platform paired with structurally engineered microfluidic plastic strips for quantitative OPA monitoring. The strips utilize a confined microfluidic geometry to achieve capillary-driven volumetric self-metering (5.4 μL), while cross-hatched micro-structures eliminate edge pooling, yielding uniform colorimetric responses. Analytically, the system integrates a matrix-matched reagent formulation, an interference-free indicator, and an automated steady-state ratiometric readout algorithm to counteract physical dilution and spectral interference. Cross-validation against a capillary electrophoresis benchmark confirmed quantitative accuracy (R^2 = 0.9684) under physical dilution of real-world CIDEX OPA solutions. This correlation facilitated a matrix-compensated 0.32% diagnostic threshold for unambiguous, automated "[PASS]" or "[FAIL]" alerts. Ultimately, this scalable, cost-effective microfluidic architecture provides an objective point-of-care diagnostic solution, demonstrating translational potential for broad dry chemistry optical detection.

Keywords: point-of-care testing (POCT); endoscope reprocessing; dry chemistry; ratiometric analysis; high-level disinfection (HLD); edge pooling

1. Introduction

Flexible endoscopes are indispensable instruments in modern clinical diagnostics and minimally invasive therapeutic procedures. Because these devices contain long and complex internal channels and are repeatedly reused between patients, inadequate reprocessing may lead to microbial contamination and subsequent healthcare-associated infections [1–3]. Several reports have documented infection transmission associated with improperly disinfected endoscopes, emphasizing the need for strict high-level disinfection (HLD) during routine clinical practice [2–5]. Among currently available HLD agents, *ortho*-phthalaldehyde (OPA) has become one of the most widely used disinfectants for endoscope reprocessing due to its strong antimicrobial efficacy, lower vapor toxicity compared with glutaraldehyde, and improved compatibility with medical device materials [6–8]. Commercial OPA disinfectant formulations typically contain approximately 0.55% (*w*/*v*) OPA, which can maintain efficacy through repeated reprocessing cycles provided that the

Check for updates

Received: 23 May 2026
Revised: 19 June 2026
Accepted: 21 June 2026
Published: 24 June 2026

Copyright: © 2026 by the authors. Licensee MDPI, Basel, Switzerland. This article is an open access article distributed under the terms and conditions of the Creative Commons Attribution (CC BY) license.

active concentration strictly remains above the minimum effective concentration (MEC) of approximately 0.30% [9]. During repeated use, however, the effective OPA concentration gradually decreases. This decline arises primarily from chemical consumption by organic contaminants (e.g., residual proteins) on medical instruments, as well as physical dilution caused by residual rinse water introduced during the pre-cleaning stage [10]. Because these processes progressively reduce disinfectant activity, clinical guidelines mandate the routine monitoring of OPA concentration prior to each disinfection cycle to ensure that the disinfectant remains above the MEC threshold [6,11].

Currently, verification of OPA disinfectant activity in hospitals is commonly performed using disposable colorimetric indicator strips, which provide a rapid and convenient estimation of disinfectant concentration through visually interpreted color changes [12]. However, these strips generally provide only semi-quantitative measurements, as the results rely on subjective visual comparison with reference color charts, which may introduce inter-observer variability. In addition, the results may be influenced by practical factors such as sample absorption variability, strict timing requirements, and environmental storage conditions [13,14]. As a result, conventional indicator strips are mainly designed to provide approximate concentration estimates rather than quantitative measurements of OPA concentration.

To improve analytical accuracy, various laboratory-based analytical methods have been developed for quantitative determination of OPA and other aldehyde compounds. High-performance liquid chromatography (HPLC), spectrophotometric derivatization techniques, and electrochemical detection strategies have demonstrated high sensitivity and selectivity for aldehyde analysis [7,12,14–17]. Although these techniques provide excellent analytical performance, they typically require sophisticated instrumentation and trained personnel, which limits their applicability in routine hospital environments where rapid on-site verification is required.

Recent advances in portable chemical sensing technologies have enabled the development of miniaturized analytical platforms capable of performing rapid on-site measurements. In particular, paper-based microfluidic analytical devices (μPADs) and strip-based sensors have attracted attention due to their low cost, simple fabrication, and minimal reagent consumption [18,19]. Integration of optical detection with these platforms has enabled quantitative chemical analysis using compact readers or smartphone-based imaging systems [20–22]. Despite these advantages, conventional porous substrates may exhibit irregular fluid flow, heterogeneous reagent distribution, and air bubble entrapment within reaction regions. These effects can lead to non-uniform color development and introduce signal variability in optical detection systems, thereby limiting measurement reproducibility [18,19].

To address these limitations, this study proposes a structurally engineered microfluidic plastic strip and a companion portable multi-spectral sensing platform for the quantitative determination of OPA concentrations. The test strip incorporates cross-hatched micro-structures to achieve volumetric self-metering and eliminate edge pooling, ensuring uniform color development. Analytically, the system integrates a matrix-matched reagent formulation, an interference-free colorimetric indicator, and an automated steady-state ratiometric readout algorithm. This combined architecture overcomes common clinical pitfalls, including sample matrix dilution, spectral interference from disinfection byproducts, and operator-dependent timing errors. Cross-validated against a capillary electrophoresis (CE) reference standard using real-world CIDEX OPA solutions, the developed platform provides an objective, real-time “[PASS]” or “[FAIL]” digital output, offering a reliable diagnostic tool for routine endoscope reprocessing workflows.

2. Materials and Methods

2.1. Chemicals and Reagents

o-Phthalaldehyde (OPA), disodium hydrogen phosphate, sodium dihydrogen phosphate, sodium tetraborate (borax), sodium hydroxide, hydrochloric acid, and sodium dodecyl sulfate (SDS) were purchased from Nacalai Tesque (Kyoto, Japan). Glycine, methanol, Tween-20, and polyvinylpyrrolidone (PVP-360, MW: 360,000) were obtained from Sigma-Aldrich (St. Louis, MO, USA). Phenolphthalein disodium salt was obtained from Tokyo Chemical Industry Co. (Tokyo, Japan). Sodium sulfite and citric acid monohydrate were obtained from Wako Pure Chemical Industries (Osaka, Japan). Tris (hydroxymethyl)aminomethane hydrochloride was purchased from Thermo Scientific (Waltham, MA, USA). All chemicals and reagents were of analytical grade and used as received without further purification. The commercial OPA disinfectant (CIDEX™ OPA Solution) and chemical test strips (CIDEX™ OPA Solution Test Strips) were purchased from Advanced Sterilization Products (Irvine, CA, USA). Ultrapure water ($\geq$18.2 MΩ·cm), prepared using a Direct-Q gradient system (Millipore, Burlington, MA, USA), was used throughout the experiments.

2.2. Preparation of OPA Standard Solutions, Real Samples, and Derivatized Mixtures

A 100 mM phosphate buffer (PB, pH 7.4) was prepared using deionized water and stored at room temperature. A 10% (*w*/*v*) OPA stock solution was prepared by dissolving 0.1 g of OPA in 1 mL of 99% methanol. The 10% OPA stock was freshly diluted with 35 mM PB (pH 7.4) to yield a 1% (*w*/*v*) intermediate solution, which was subsequently diluted with the same buffer to obtain final OPA standard working solutions ranging from 0.025% to 0.55% (*w*/*v*).

Real clinical samples were prepared by directly diluting the commercial CIDEX OPA stock solution with deionized (DI) water to achieve the desired concentration ranges (e.g., 0.24–0.40%, *w*/*v*) according to the manufacturer's guidelines [23]. For derivatization, 0.20% (*w*/*v*) OPA was reacted with 3 mM glycine in 35 mM PB (pH 7.4). UV-Vis absorption spectra were recorded using a Jasco V-730 spectrophotometer (JASCO, Tokyo, Japan) equipped with a 1 mm path length quartz cuvette.

2.3. Preparation of Colorimetric Sensing Reagent

The coating solution was prepared at a three-fold (3X) concentration in a 30 mM borax buffer (pH 9.2) containing 6.0% (*w*/*v*) polyvinylpyrrolidone (PVP-360), 0.09% Tween-20, 210 mM Na_2SO_3, and 7.5 mM phenolphthalein disodium salt. The mixture was dissolved via vigorous vortex mixing and stored at room temperature prior to deposition onto the patterned microfluidic test strips.

2.4. Fabrication of the Patterned Microfluidic Test Strips

The multi-layered colorimetric test strips were assembled utilizing a reproducible lamination process. As illustrated in the schematic architecture (Figure 1A), the five-layer structure was precisely dimensioned and patterned using a Silhouette CAMEO 3 cutting machine (Silhouette America, Lindon, UT, USA) equipped with an AutoBlade (Type A). The structural foundation of the reaction zone consisted of a middle white polyethylene terephthalate (PET) film (HY21, 250 μm thickness; Nan Ya Plastics Corp., Taipei, Taiwan). Prior to assembly, the surface of this middle PET film was scored by the same cutting machine to create a 0.2 mm × 0.2 mm crosshatch grid pattern (cutting parameters: depth = 1, force = 20) exclusively within the designated reaction areas. The surface topography and depth of this patterned micro-structure were characterized using a 3D surface profiler (VK-

3000 series, KEYENCE, Osaka, Japan) equipped with a 10× objective lens and a 404 nm violet laser source (Figure 1B).

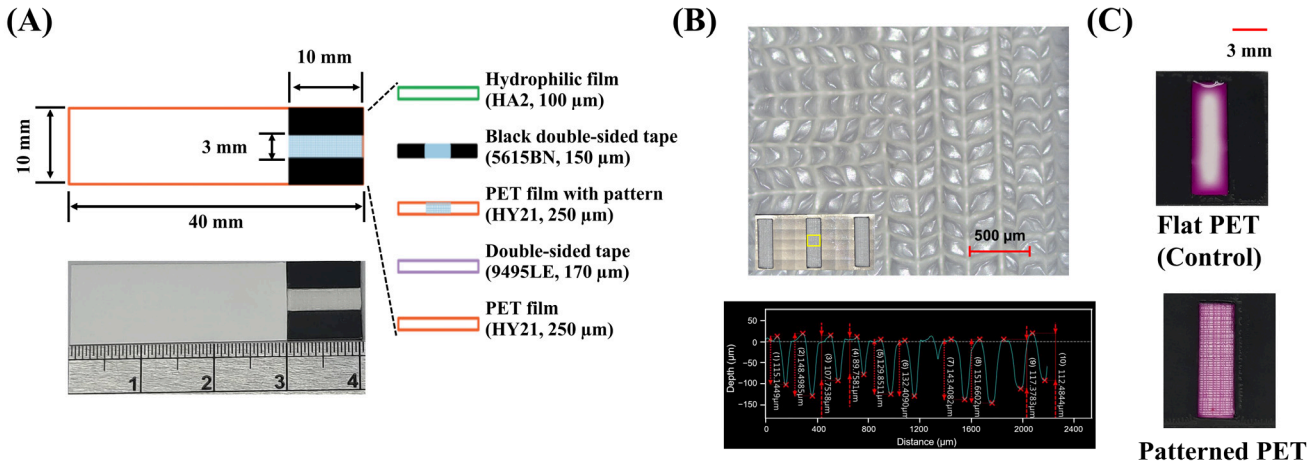

Figure 1. The design and surface topography of the patterned microfluidic test strip. (**A**) Schematic illustration and photograph of the assembled multi-layered test strip. (**B**) Optical micrograph and the corresponding depth profile of the cross-hatched micro-structures on the patterned PET film. (**C**) Comparison of reagent deposition on flat and patterned PET films. To visualize the fluidic behavior prior to drying, 1.8 µL of a freshly prepared 3X concentrated formulation—comprising 15 mM borax (pH 10.0), 6.0 mM phenolphthalein disodium salt, 210 mM Na_2SO_3, 0.09% Tween-20, and 6.0% PVP-360—was dispensed into the reaction zones. This specific pH 10.0 condition was deliberately utilized to present a distinct dark red color for enhanced macroscopic observation.

A pre-cut black double-sided adhesive tape (5615BN, 150 µm thickness; Nitto, Osaka, Japan) was aligned and laminated onto the patterned middle PET film using a custom-designed jig, with an alignment error within 0.2 mm. This black tape featured rectangular cutouts (10 mm × 3 mm) to strictly confine the applied reagent and serve as an optical boundary. Subsequently, an aliquot of 1.8 µL of the freshly prepared 3X colorimetric sensing reagent was dispensed into each defined reaction zone.

The partially assembled strips were then dried in an oven at 50 ± 2 °C for 60 s to completely solidify the reagent. Following solvent evaporation, the protective liner of the black tape was peeled off, and a hydrophilic functional plastic cover film (HA2, 100 µm thickness; E-Miracle Composite Corp., Hsin-Chu, Taiwan) was laid over the tape to seal the reaction zones and provide fluidic wicking guidance. Finally, a supporting double-sided tape (9495LE, 170 µm thickness; 3M, St. Paul, MN, USA) and a rigid white PET base substrate (HY21, 250 µm thickness) were sequentially applied to the bottom of the middle PET film, yielding individual test strips with overall dimensions of 40 mm × 10 mm (Figure 1A). This standardized lamination process and precise microfluidic topography ensure high batch-to-batch fabrication reproducibility, thereby further strengthening the translational value of the developed sensor.

2.5. Design of Multi-Spectral Optical Detection Platform

A custom-built, miniaturized optical detection platform with compact physical dimensions of 78 mm (L) × 59 mm (W) × 55 mm (H) was engineered based on the principle of reflectance photometry [24]. As illustrated in the functional block diagram (Figure 2A), the system architecture is systematically divided into four primary modules: a power supply unit (Block 1), a reaction and optoelectronic unit (Block 2), a signal processing and control unit (Block 3), and a user interface with peripherals (Block 4). The entire system is powered by Block 1, consisting of a rechargeable battery pack (two 14500 lithium-ion batteries connected in series). This pack is located in the battery compartment (Figure 2B(5)), delivering

a stable 7.4 V DC input, and is operated via a main power switch located at the side of the device (Figure 2B(5-1)).

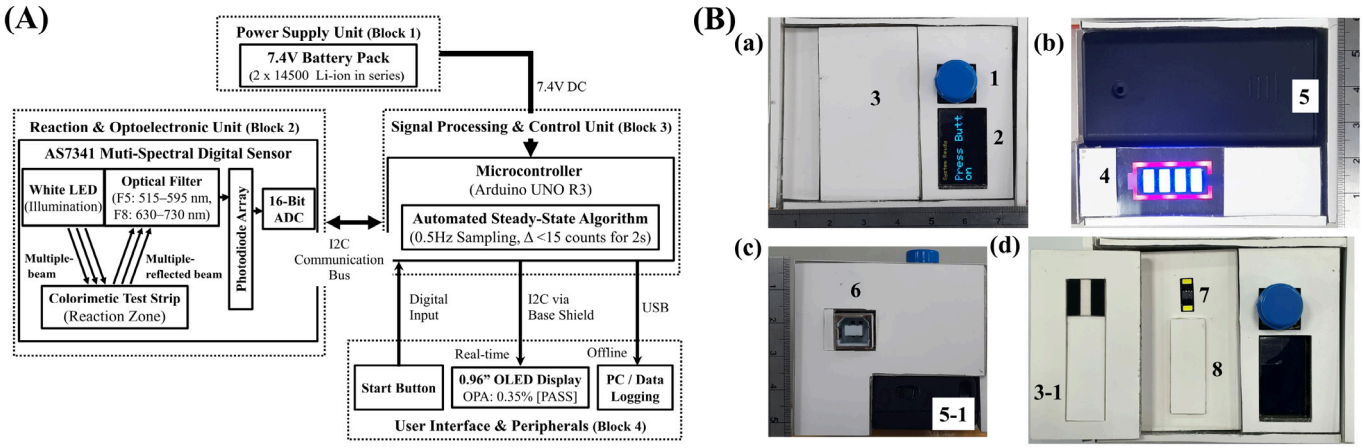

Figure 2. System architecture and physical prototype of the portable automated colorimetric sensor. (**A**) A functional block diagram illustrating the integration of the four primary hardware and software modules. (**B**) Photographs of the prototype: (**a**) Top view showing the customized strip holder (3), OLED display (2), and start button (1). (**b**) Bottom view displaying the battery compartment (5) and battery level indicator (4). (**c**) Side view presenting the main power switch (5-1) and USB port (6). (**d**) Internal view revealing the removable strip holder (3-1), the AS7341 multi-spectral sensor located between the dual built-in white LEDs (7), and the precise strip alignment fixture (8).

The optoelectronic core (Block 2) utilizes an 11-channel multi-spectral digital sensor module (AS7341, ams AG, Premstaetten, Austria), centrally positioned between dual surface-mount (SMT) white light-emitting diodes (LEDs) (Figure 2B(7)). A custom magnetic sealing mechanism was engineered. Specifically, neodymium (NdFeB) strong magnets, featuring a surface magnetic field of approximately 2400 ± 10% Gauss, are embedded within the main device body, directly behind the internal optical measurement region (i.e., beneath the white LEDs and the strip alignment fixture, Figure 2B(7,8)). These embedded magnets tightly attract an iron plate (400 µm thickness) integrated within the removable cover of the strip holder (Figure 2B(3-1)). Upon closure, this magnetic engagement creates a light-tight environment during optical reading. As revealed in the internal top view, the optical measurement region incorporates a precise strip alignment fixture (Figure 2B(8)) designed to ensure reproducible spatial positioning of the test strip. During measurement, these dual LEDs illuminate the reaction zone, with their driving current regulated via software configuration to maintain consistent illumination intensity. The diffusely reflected multiple-beam light is subsequently captured by a photodiode array and selectively monitored using the F5 channel (515–595 nm) and the F8 channel (630–730 nm). The optical signals are digitized by an internal 16-bit analog-to-digital converter (ADC) and transmitted via an I^2C communication bus. The integration time (t_{int}) is parameterized using the register values ATIME and ASTEP, defined as t_{int} = (ATIME + 1) × (ASTEP + 1) × 2.78 µs. By configuring ATIME to 29, ASTEP to 599, and the analog gain (AGAIN) to 7, the full-scale ADC output was defined at 18,000 counts.

A customized automated steady-state detection algorithm was embedded within the Arduino UNO R3 microcontroller (Arduino, Ivrea, Italy) (Block 3). Upon activation via the start button (Figure 2B(1)) through a digital input, the algorithm continuously acquires the optical responses of both the F5 and F8 channels at a sampling frequency of 0.5 Hz (i.e., one measurement every 2 s). The rate of signal variation (Δ) is calculated by comparing the current reading with the value from the preceding sampling point. A steady-state condition

is recognized when the absolute variations for both channels are minimal ($|\Delta F5| < 15$ and $|\Delta F8| < 15$). This stability criterion must be continuously satisfied for three consecutive counts.

Once the steady-state threshold is satisfied, the stabilized optical signals are computationally translated into the corresponding OPA concentration. The user interface and peripherals (Block 4) include a 0.96-inch OLED display (Figure 2B(2)), interfaced with the microcontroller via an I^2C port on a Base Shield using a Grove cable. The calculated OPA concentration is presented on the OLED screen, accompanied by a "[PASS]" or "[FAIL]" qualitative judgment based on an adjusted clinical minimum effective concentration (MEC) threshold. Additionally, the device features a real-time battery level indicator (Figure 2B(4)) to monitor power capacity and prevent unexpected operational interruptions during field applications. A USB Type-B port (Figure 2B(6)) is provided on the side panel to facilitate optional offline PC data logging.

2.6. Capillary Electrophoresis Conditions for OPA Determination

A temperature-controlled (25 °C) capillary electrophoresis system (G1600A, Agilent Technologies, Santa Clara, CA, USA), operated by 3D-CE ChemStation™ software (version B.04.03), was used for the analysis. An uncoated fused-silica capillary (Beckman Coulter, Brea, CA, USA; total length 48.0 cm, effective length to the detector 39.5 cm, 50 µm i.d., 375 µm o.d.) was flushed with 0.1 N NaOH for 40 min and then with deionized water for 20 min prior to initial use. The running buffer consisted of 20 mM sodium tetraborate and 20 mM sodium dodecyl sulfate (SDS) adjusted to pH 9.20 [25,26]. Prior to analysis, all separation buffers were degassed by sonication (40 kHz, 10 W/L, T760DH, Elmer, Taipei, Taiwan) at room temperature for 5 min.

Before each injection, the capillary was preconditioned by rinsing sequentially with 0.1 N NaOH for 1 min, deionized water for 1 min, and the running buffer for 2 min. The sample was injected hydrodynamically at 30 mbar for 5 s, followed by a short injection of the running buffer at 30 mbar for 1 s to minimize sample loss. The electrophoretic separation was performed at an applied voltage of +20 kV. Analytes were monitored using a photodiode array (PDA) detector at 200, 260, 300, 400, and 500 nm, with representative electropherograms extracted at 260 nm. After each electrophoretic run, the capillary was flushed with deionized water for 2 min.

3. Results and Discussion

3.1. Chemical Sensing Mechanism, Matrix-Matching Strategy, and Indicator Selection

The colorimetric sensing mechanism of the proposed micro-structured plastic strip aligns with the established chemical principles utilized in commercial CIDEX™ OPA Solution Test Strips. The detection is based on a nucleophilic addition reaction wherein *ortho*-phthalaldehyde (OPA) reacts with sodium sulfite (Na_2SO_3) within the reagent pad to form a sulfite addition product [27]. As detailed in Equation (1), this stoichiometric reaction generates an equivalent amount of base (sodium hydroxide, NaOH).

$$C_6H_4(CHO)_2 + 2Na_2SO_3 + 2H_2O \rightarrow C_6H_4(CH(SO_3Na)OH)_2 + 2NaOH \quad (1)$$

The localized generation of NaOH elevates the microenvironmental pH on the test strip, which subsequently triggers a deprotonation and colorimetric transition in a selected pH-sensitive indicator dye, as simplified in Equation (2).

$$\text{NaOH} + \text{pH-sensitive dye (Protonated)} \rightarrow \text{Deprotonated dye (Color shift)} \quad (2)$$

Given that this colorimetric transition is dependent on the NaOH-induced pH shift, the initial pH and the buffering capacity (i.e., PB concentration) of the sample solution govern

the quantitative accuracy of the optical readout. Because the reaction yields two moles of NaOH for every mole of OPA consumed, overcoming the inherent buffer capacity of the disinfectant is a critical factor in sensing design. The baseline chemical matrix was characterized via acid-base titration of three independent batches of fresh CIDEX™ OPA Solution (0.55% OPA). The results confirmed a consistent baseline chemical environment, characterized by a pH of 7.4 and a PB concentration of 42–44 mM.

However, in actual clinical reprocessing workflows, a primary mechanism driving the reduction in OPA concentration from its initial 0.55% level towards the 0.30% minimum effective concentration (MEC) is physical dilution caused by residual rinsing water inside the pre-cleaned endoscopes. This physical dilution proportionally reduces the intrinsic buffering capacity of the disinfectant. Accurate quantification of real-world samples necessitates minimizing the matrix discrepancy between the standard calibration solutions and the actual clinically diluted samples. Consequently, a customized 35 mM phosphate buffer (PB, pH 7.4) was strategically selected as the universal matrix for all OPA standard solutions (0.025–0.55%), rather than calibrating against the original 44 mM PB matrix. This 35 mM PB concentration corresponds to the buffering capacity of a physically diluted 0.45% CIDEX OPA solution—a representative mid-upper value within the critical 0.30–0.55% clinical working range. By anchoring the standard calibration curve to this specific mid-point matrix, the maximum deviation in buffer capacity between the calibration standards and any clinically diluted sample is minimized. This matrix-matching strategy ensures quantitative accuracy and reliable colorimetric readout across the practical disinfection window.

In addition to physical dilution, OPA concentration also decreases via chemical consumption by residual proteins. A derivatization approach introducing glycine was employed to simulate the depletion of active OPA during the actual CIDEX™ OPA disinfection process. As depicted in Figure 3A, the unreacted OPA standard solution was characterized by an absorption peak at 260 nm, possessing no significant optical activity above 350 nm. This 260 nm peak was thus established as the quantitative monitoring wavelength for the subsequent CE analysis. Following the introduction of 3 mM glycine, rapid derivatization was optically and visually observed. Within 0.5 min, the reaction yielded a noticeable yellow-green hue, simultaneous with the emergence of a broad absorption band at 400 nm characteristic of the newly formed isoindole derivatives. Over the incubation period, the continuous generation of these derivatives was evidenced by a progressive rise in the 400 nm absorbance [27,28]. Notably, by the 5 min mark, the mixture had transitioned to a deep green color, and the upward trajectory of the 400 nm absorbance began to plateau, reflecting a deceleration in the reaction kinetics as the derivatization proceeded. From a quantitative sensing perspective, this prolonged and non-linear kinetic behavior renders the 400 nm optical readout highly time-dependent. Because the generation rate of the reaction products varies significantly across the incubation window, any slight deviation in the specific detection time would introduce severe measurement variability, making this direct derivatization approach unsuitable for rapid and robust point-of-care testing.

The UV-Vis spectra (Figure 3A) also demonstrated that the OPA-glycine isoindole derivatives exhibit no significant optical absorption at wavelengths above 500 nm. This optical property served as a fundamental criterion for the design of the chemical test strips. Circumventing spectral overlap and visual interference from the dark-green disinfection byproducts requires the target absorption shift of the colorimetric pH indicator to occur exclusively at wavelengths greater than 500 nm. Consequently, phenolphthalein disodium salt was selected as the pH indicating component for the test strips. As further demonstrated in Figure 3B, the pH-dependent UV-Vis absorption spectra of 0.5 mM phenolphthalein disodium salt in a 20 mM borax buffer display a progressive deprotonation

and colorimetric transition across an alkaline pH range from 8.60 to 10.0. This transition is characterized by the emergence of a dominant absorption peak near 555 nm, which aligns with the >500 nm requirement, ensuring an interference-free optical readout during practical disinfection monitoring.

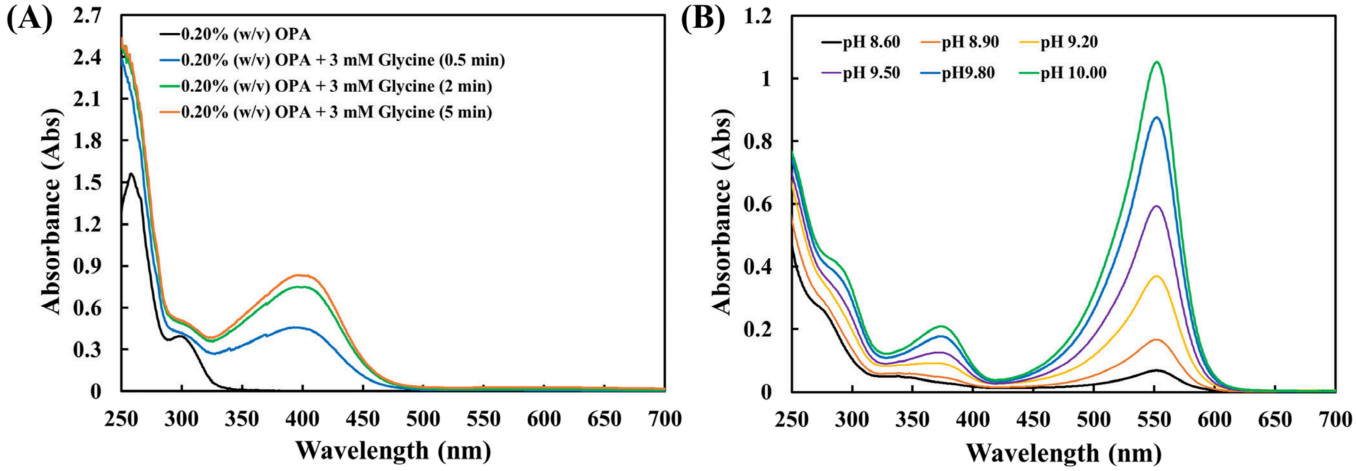

Figure 3. UV-Vis absorption spectra of the colorimetric sensing components. (**A**) Time-dependent spectra of 0.20% (*w*/*v*) OPA reacting with 3 mM glycine in 35 mM PB (pH 7.4), demonstrating the characteristic peak of isoindole derivatives near 400 nm. (**B**) pH-dependent spectra of 0.5 mM phenolphthalein in 20 mM borax buffer, showing the progressive colorimetric transition near 555 nm across a pH range of 8.60 to 10.0. All measurements were performed using a 1 mm path length quartz cuvette.

Furthermore, as revealed in Figure 3B, the absorbance of the phenolphthalein indicator exhibits a steep increase particularly within the pH window of 8.90 to 10.0. By precisely calibrating the initial buffer capacity of the system, the stoichiometric generation of NaOH resulting from the targeted 0.28–0.40% OPA reaction (Equation (1)) elevates the microenvironmental pH into this responsive window. This alignment between the OPA-induced pH shift and the indicator's dynamic colorimetric range establishes an optimal detection interval that encompasses the critical 0.30% MEC, thereby ensuring reliable clinical decision-making during practical disinfection monitoring.

3.2. Microfluidic Topography Design and Volumetric Self-Metering of the Test Strip

The architectural design of the test strip plays a crucial role in maintaining fluidic stability and optical precision. As illustrated in the structural schematic (Figure 1A), the optical measurement zone was confined to 10 mm in length and 3 mm in width using a precise cutout in the black double-sided adhesive tape. This 3 mm width was established as a critical geometric constraint. Experimental observations revealed that maintaining the reaction zone width below 6 mm is essential to ensure a uniform and steady advancing flow front. Exceeding this dimensional threshold creates a flow velocity disparity between the faster lateral edges and the slower central region, leading to the entrapment of air bubbles in the center of the channel, interfering with the multi-spectral reflectance measurements. Similarly, the vertical dimension—defined by the thickness of the black double-sided tape—was optimized. A spacer thickness below 50 μm generated excessive fluidic resistance, while exceeding 200 μm caused disparity in fluid advancing speeds and microbubble entrapment. Therefore, a commercially available 150 μm thickness was selected to prevent bubble formation while maximizing the optical reaction volume, thereby enhancing the overall sensitivity of the test strip.

Beyond the macroscopic channel dimensions, a homogeneous reagent distribution is fundamental for reliable colorimetric sensing. When dissolved reagents are deposited into the confined reaction zone on conventional flat substrates, surface tension causes the liquid to form a meniscus against the tape boundaries. This leads to the immediate outward migration and edge pooling of the liquid reagent, as observed on the wet flat PET film (Figure 1C, top). Upon thermal drying, this physical boundary pins the contact line, solidifying and culminating in a surface-tension-driven peripheral pooling of the dried reagents. To overcome this phenomenon, a 0.2 mm × 0.2 mm cross-hatched micro-structure was patterned onto the surface of the middle PET substrate. As characterized by the surface profiler (Figure 1B), this topographical modification creates physical micro-cavities with depths ranging from approximately 80 to 150 μm.

During the initial liquid deposition phase, the freshly dispensed reagent (which exhibits a visibly deeper color prior to drying due to the highly alkaline formulation at pH 10.0) can be observed distributing uniformly within these micro-grooves without edge pooling (Figure 1C, bottom). However, upon thermal drying, the deprotonated phenolphthalein naturally reverts to a colorless state, making macroscopic observation of the solid reagent challenging. Therefore, a distinctively colored surrogate dye (thymol blue sodium salt) was utilized to verify this homogeneous spatial distribution after drying. As visually confirmed in Figure A1, the light-yellow dried solid reagents remain uniformly sequestered at the bottom of these micro-cavities. Furthermore, during sample introduction, these micro-structures effectively buffer the solid reagent surface from the direct impact of the laterally flowing liquid, thereby preventing reagent washout. As a result, the patterned PET substrate eliminates this surface-tension-driven pooling effect, yielding a uniform color development across the entire reaction zone.

This engineered micro-topography also serves as the mathematical foundation for the quantitative formulation of the colorimetric sensing reagent. The total volumetric capacity of the reaction zone determines the dilution factor of the pre-coated reagents upon sample reconstitution. Based on the spatial geometry, the rectangular void of the black tape (10 mm length × 3 mm width × 0.15 mm thickness) provides a base volume of 4.5 μL. Combined with an estimated 0.9 μL fluidic capacity from the underlying micro-cavities (derived via gravimetric measurement of absorbed deionized water), the reaction zone yields a total sample-holding volume of 5.4 μL. Therefore, to dynamically achieve the optimal 1× working concentration when the 5.4 μL sample fills the zone, the 1.8 μL of dispensed reagent must be prepared at 3.0 times (5.4 μL/1.8 μL) the final target concentration. This 3× formulation ensures consistent chemical stoichiometry and reproducible optical responses during actual clinical monitoring. Unlike commercial paper-based test strips, whose absorbed sample volume is inherently variable and dependent on operator handling (e.g., dipping time and angle), this fully enclosed microfluidic architecture guarantees the precise, automatic uptake of a fixed 5.4 μL OPA sample. This quantitative, self-metering design eliminates user-induced volumetric fluctuations, thereby elevating the analytical precision and reliability of the colorimetric assay.

3.3. Hardware Architecture and Automated Steady-State Readout Algorithm

To translate the chemical colorimetric transition into a quantifiable digital signal, the sensing platform utilizes the AS7341 multi-spectral sensor. Based on the optical characterization of the phenolphthalein indicator (established in Section 3.1), the F5 channel (515–595 nm) was selected as the primary measurement channel, as its detection band encompasses the 555 nm absorption peak of the deprotonated dye. Simultaneously, the F8 channel (630–730 nm) was designated as an optical reference to compensate for background optical scattering and inherent fluctuations in the internal LED emission intensity,

thereby enabling the derivation of a robust analytical optical ratio (F8/F5). To empirically validate this ratiometric approach, signal stability was systematically evaluated. To ensure consistency with the baseline conditions of the dynamic optical response depicted in Figure 4A, this evaluation was conducted using a 0.32% (*w*/*v*) OPA sample in 35 mM PB, paired with test strips containing a final effective matrix of 5 mM borax (pH 9.2), 2.0 mM phenolphthalein disodium salt, 70 mM Na_2SO_3, 0.03% Tween-20, and 2.0% PVP-360. As detailed in Table 1, while the individual F5 and F8 channels exhibited signal fluctuations due to background optical scattering and subtle positional variations, employing the F8/F5 optical ratio effectively canceled out these common-mode interferences. Consequently, the coefficient of variation (CV) of the final ratiometric readout was reduced to 1.46%. This enhancement in signal precision confirms that the F8/F5 ratio minimizes optical and positional interferences, providing a reliable quantitative foundation for the colorimetric assay.

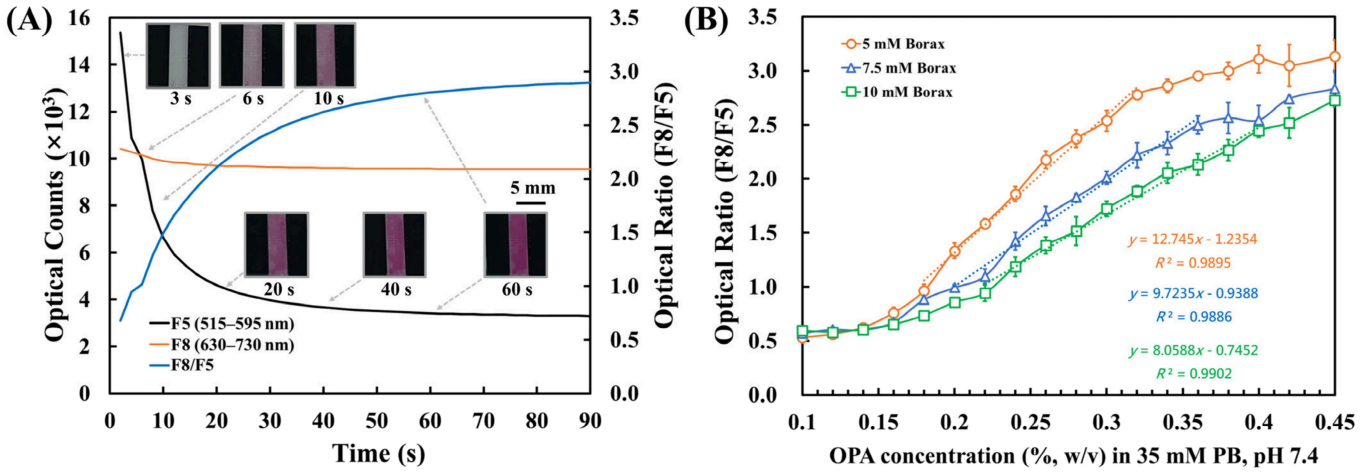

Figure 4. Dynamic optical response and parameter optimization of the colorimetric sensor. (**A**) Real-time optical counts (F5 and F8 channels) and the calculated F8/F5 ratio for a 0.32% (*w*/*v*) OPA sample in 35 mM PB (pH 7.4). The plotted dynamic response represents a test strip formulated with a final effective matrix of 5 mM borax (pH 9.2), 2.0 mM phenolphthalein disodium salt, 70 mM Na_2SO_3, 0.03% Tween-20, and 2.0% PVP-360. Inset photographs show the corresponding macroscopic color development over 60 s. (**B**) Calibration curves of the F8/F5 ratio versus OPA concentrations (0.10–0.45%, *w*/*v*) under varying borax buffer concentrations (5, 7.5, and 10 mM). The base reagent formulation was maintained identical to (**A**), with only the borax concentration varied. Dotted lines indicate linear dynamic ranges. Error bars represent standard deviations (n = 5).

Table 1. Signal stability evaluation of individual optical channels and ratiometric readout from five independent measurements (0.32% *w*/*v* OPA in 35 mM PB).

Measurement No.	Primary Channel F5 (Counts)	Reference Channel F8 (Counts)	Optical Ratio (F8/F5)
1	3574	9956	2.786
2	3140	8854	2.820
3	3776	10527	2.788
4	3542	9895	2.794
5	3455	9367	2.711
Mean	3497	9720	2.780
Standard Deviation (SD)	231.84	634.85	0.041
Coefficient of Variation (CV, %)	6.63	6.53	1.46

The real-time kinetic response of the test strip was evaluated. When the tip of the microfluidic strip contacts the OPA sample, the fluid is rapidly wicked into the reaction zone via capillary action. Notably, within 1–2 s, the synergistic hydrophilicity of the top functional cover film and the underlying PVP-360 polymer matrix bidirectionally drives the sample, ensuring a rapid and uniform fluidic distribution across the entire microfluidic cavity. Once the reaction zone is filled, the OPA solution interacts with the sequestered reagents at the bottom of the micro-grooves, initiating the stoichiometric colorimetric reaction. As depicted in the dynamic optical response (Figure 4A), this rapid dissolution and subsequent reaction manifest as a steep decline in the F5 channel counts during the initial seconds. In contrast, the F8 reference channel remains stable throughout the entire hydration and reaction process. Consequently, the calculated optical ratio (F8/F5) exhibits a steep ascent that mirrors the reaction kinetics. The inset macroscopic photographs corroborate this dynamic behavior, revealing a distinct color transition from transparent to pink as early as 3 s after sample introduction.

In commercial paper-based test strips, the final interpretation relies on a timed visual inspection by the operator, which introduces subjective bias and temporal errors. To eliminate these uncertainties, a customized automated steady-state detection algorithm was embedded within the microcontroller (Figure 2A). Upon activation, the algorithm continuously monitors the raw optical counts of both the F5 and F8 channels at a sampling frequency of 0.5 Hz (i.e., one measurement every 2 s). To dynamically assess the reaction equilibrium, the rate of signal variation (Δ) is calculated by comparing the current reading with the preceding sampling point. A steady-state condition is recognized when the absolute variations for both channels are simultaneously minimal ($|\Delta F5| < 15$ and $|\Delta F8| < 15$). This specific threshold of 15 counts corresponds to a relative signal fluctuation of less than 1%, indicating chemical equilibrium. To prevent premature evaluation during the kinetic deceleration phase, this stability criterion must be continuously satisfied for three consecutive counts. As evidenced in Figure 4A, the raw signals progressively level off, culminating in a stable plateau for the analytical F8/F5 ratio. The system satisfies this steady-state algorithmic threshold at approximately 60 s, which coincides with the visually saturated color development observed in the corresponding 60 s inset photograph.

Upon satisfying the steady-state criterion, the stabilized F8/F5 optical ratio is processed to determine the OPA concentration. For immediate clinical decision-making, this calculated concentration is displayed on the OLED screen, accompanied by an unambiguous "[PASS]" or "[FAIL]" judgment based on a matrix-compensated diagnostic threshold of 0.32% OPA (as established in Section 3.6). This architectural and algorithmic integration ensures that the final analytical readout is objective, real-time, and reliable at the point of care.

3.4. Systematic Optimization of Reagent Formulation and Analytical Performance

To ensure uniform spatial distribution, rapid reaction kinetics, and optical performance, the formulation of the colorimetric sensing reagent was systematically optimized. Initially, polyvinylpyrrolidone (PVP-360) was incorporated not only as a film-forming and stabilizing agent but also to impart essential fluidic advantages [29,30]. Upon sample introduction, the inherent hydrophilicity of the dried PVP-360 matrix guides the OPA sample to fill the entire microfluidic reaction zone. Furthermore, during the extended optical monitoring period (conservatively covering the >90 s reaction window), PVP-360 acts as a potent humectant. It retains moisture and minimizes the water evaporation rate, thereby preserving the precisely metered 5.4 μL reaction volume. During the fabrication process, the concentration of PVP-360 in the 3X coating solution was evaluated. The experimental results indicate that a 6.0% (w/v) coating concentration—which yields a 2.0% final effective

reaction concentration upon sample rehydration—provided the optimal viscosity. Coating concentrations below 2% lacked viscosity to prevent localized reagent accumulation during thermal drying, whereas excessive concentrations (>9%) hindered uniform liquid deposition and retarded OPA diffusion and reaction kinetics. In synergy with the PVP-360 matrix, an effective concentration of 0.03% Tween-20 was introduced. This non-ionic surfactant lowers the surface tension to facilitate uniform reagent coating, stabilizes the highly concentrated phenolphthalein disodium salt, and accelerates the overall OPA colorimetric reaction. Notably, effective surfactant concentrations exceeding 0.2% were avoided, as the formation of micelles was observed to suppress the colorimetric readout.

Following the establishment of the physical polymeric matrix, the chemical reactive components were systematically evaluated. Sodium sulfite (Na_2SO_3) was established at an effective concentration of 70 mM. This concentration provides a sufficient stoichiometric excess to react with up to approximately 0.47% (35 mM) OPA, ensuring maximum generation of hydroxide ions (OH^-) for the subsequent colorimetric shift. From a practical engineering perspective, Na_2SO_3 exhibits strong reducing properties and is susceptible to rapid aerial oxidation and peroxide-induced degradation. To complement the chemical formulation with physical protection, the final fabricated test strips must be packaged in a 45 mm × 75 mm polypropylene (PP) plastic bottle equipped with 2 g of silica gel desiccant and a 30 cm^3 oxygen scavenger to ensure long-term storage stability and an extended shelf-life.

Controlling the baseline pH and buffering capacity of the dried test strip is critical. While hydrochloric acid (HCl) is conventionally added to borate solutions to fine-tune the initial pH in liquid-phase buffer preparations, its high volatility during the 50 °C thermal drying process leads to pH fluctuations and irreproducibility in the solid-state strips [31]. Therefore, HCl titration was excluded from the formulation. Instead, an unadjusted pure borax buffer system (naturally at pH 9.2) was employed. Rather than artificially forcing the initial pH with an acid, the system's performance was optimized by varying the concentration of the borax buffer to stably anchor the microenvironmental pH and counteract the intrinsic 35 mM PB background of the standardized calibration matrix. As illustrated in the preliminary calibration curves (Figure 4B), the effective borax concentration was evaluated at 5, 7.5, and 10 mM. The experimental data revealed a rightward shift and broadening of the linear dynamic range as the borax concentration increased. The linear responsive window progressively shifted from 0.18–0.32% OPA (at 5 mM borax) to 0.20–0.36% OPA (at 7.5 mM borax), and to 0.22–0.40% OPA (at 10 mM borax, R^2 = 0.9902). While a lower borax concentration (5 mM) exhibited the highest analytical sensitivity, it led to premature signal saturation. Similarly, for the 7.5 mM borax condition, as the OPA concentration approached 0.4% (Figure 4B), a fluctuating drop in the ratiometric signal was observed. Optically, under such highly saturated coloration, the F5 counts (the denominator) drop to a low baseline level, causing any minute physical fluctuations to be mathematically amplified in the F8/F5 calculation. This amplification effect fundamentally explains the increased error bars and the fluctuating drop of the ratiometric signal. Conversely, the 10 mM borax condition broadened the dynamic range to encompass the targeted clinical requirement, ensuring sufficient analytical resolution within the critical 0.30% to 0.40% OPA monitoring window. Furthermore, an evaluation of the system's reproducibility revealed that the inherent error (standard deviation) of the F8/F5 ratio is consistently less than 0.08 (n = 5). For the 10 mM borax condition, the linear regression slope is approximately 8.0, mathematically implying that a 0.01% variation in OPA concentration yields a proportional 0.08 shift in the optical ratio. Under this condition, the sensor retains adequate discriminability and resolution. If the borax concentration were increased any further, the slope would drop below this critical threshold, failing to provide

sufficient resolution against the intrinsic signal variance. Therefore, 10 mM borax was selected as the optimal buffering matrix.

Finally, to compensate for the suppressed slope and elevate the resolving power under the 10 mM borax condition, the phenolphthalein indicator concentration was fine-tuned from 2.0 mM to 2.5 mM. This strategic elevation amplified the specific optical absorbance upon deprotonation, ultimately maximizing the sensitivity of the test strip. Under these optimal reagent conditions (2.5 mM phenolphthalein disodium salt, 10 mM borax, 70 mM Na_2SO_3, 0.03% Tween-20, and 2.0% PVP-360), the overall analytical performance of the sensing platform was comprehensively evaluated (Figure 5). The customized sensor demonstrated a reliable linear response (R^2 = 0.9956) across the targeted OPA concentration window (0.26–0.40%). More importantly, as visually corroborated by the inset macroscopic photographs in Figure 5, the test strips exhibited a vivid, easily distinguishable colorimetric progression—transitioning from a faint pink at 0.14% to a deep, saturated magenta at 0.40%. This progressive visual color development synchronizes with the quantified F8/F5 optical ratio, providing a dual-mode (visual and digital) verification. Crucially, the optimized linear dynamic range encompasses the critical 0.30% minimum effective concentration (MEC) and its surrounding clinical monitoring window. This precise alignment empowers the automated steady-state algorithm to execute accurate "[PASS]" or "[FAIL]" clinical judgments, thereby minimizing the risk of false diagnostics during routine endoscope reprocessing.

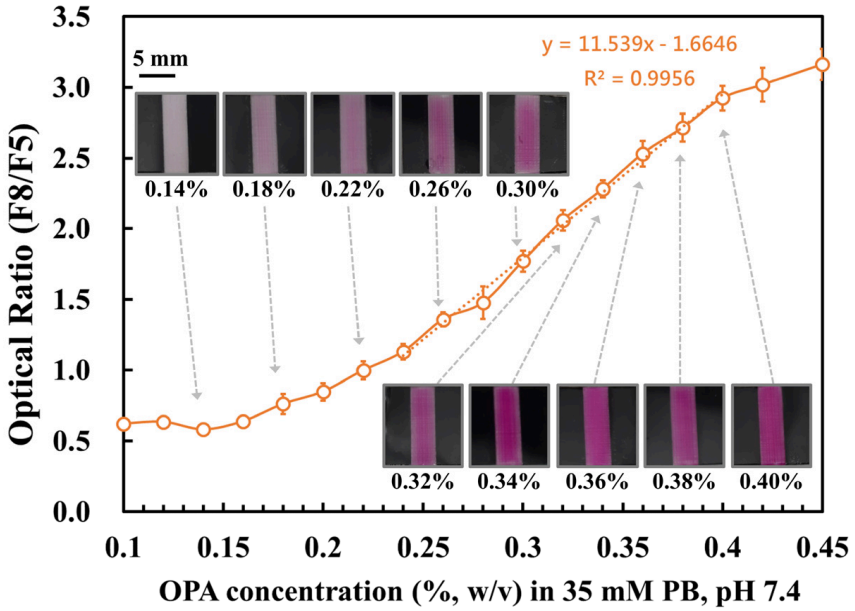

Figure 5. The calibration curve and colorimetric response under optimal reagent conditions. The curve plots the optical ratio (F8/F5) against OPA concentrations (0.10–0.45%, *w*/*v*) in 35 mM PB (pH 7.4). The test strips were formulated to yield a final optimal effective matrix comprising 2.5 mM phenolphthalein disodium salt, 10 mM borax (pH 9.2), 70 mM Na_2SO_3, 0.03% Tween-20, and 2.0% PVP-360. Inset photographs display the progressive macroscopic color development of the test strips across OPA concentrations (0.14–0.40%). The dotted line indicates the linear regression fit. Error bars represent standard deviations (n = 5).

3.5. Establishment of Capillary Electrophoresis as Reference Benchmark

To evaluate the quantitative accuracy and reliability of the developed microfluidic colorimetric sensor, capillary electrophoresis (CE) was employed as an independent, standard reference method. Under the optimized electrophoretic conditions (20 mM sodium tetraborate and 20 mM SDS at pH 9.20) [25,26], the migration of the OPA molecule was

monitored using a photodiode array (PDA) detector at its characteristic 260 nm absorption wavelength, a quantitative spectral feature previously established in Section 3.1.

As depicted in the representative electropherograms (Figure 6A), the electrophoretic separation was efficient. The 0.55% OPA standard solution (trace a) exhibited a well-defined analyte peak (Peak 1) at a migration time of approximately 2.9 min, achieving a separation efficiency with a theoretical plate number (*N*) exceeding 50,000. The system also exhibited reproducibility, as evidenced by a coefficient of variation (CV) for the migration time of less than 0.35%. When analyzing the complex commercial 0.55% CIDEX OPA solution (trace b), the CE method achieved baseline separation between the primary OPA analyte and other fundamental formulation additives. Notably, benzotriazole (Peak 2), which is commonly utilized as a corrosion inhibitor in commercial endoscopic disinfectants [32], was resolved at a migration time of approximately 5.4 min. This baseline resolution demonstrates that the established CE methodology is free from sample matrix interference, ensuring the analytical specificity required for a reference standard.

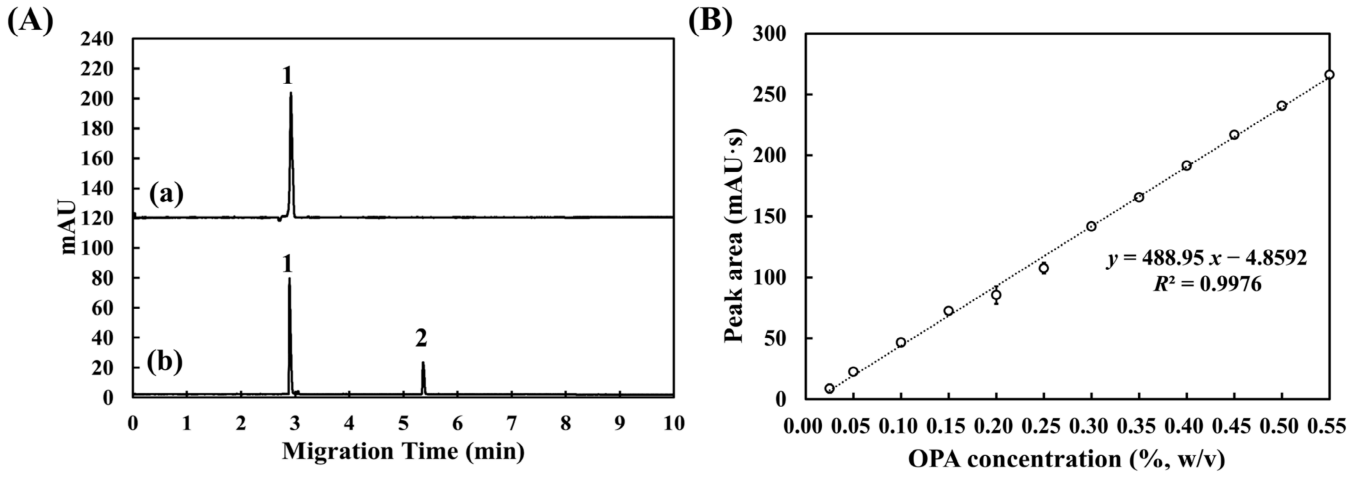

Figure 6. Capillary electrophoresis (CE) analysis and calibration curve of OPA. (**A**) Electropherograms of (**a**) 0.55% OPA standard in 35 mM PB (pH 7.4) and (**b**) 0.55% CIDEX OPA solution. Peak identification: 1, OPA; 2, benzotriazole. Separations were conducted using a running buffer of 20 mM sodium tetraborate containing 20 mM SDS (pH 9.20) with UV detection at 260 nm. (**B**) Calibration curve of OPA standards (0.025–0.55%, *w*/*v*) with a linear regression fit (R^2 = 0.9976). Error bars represent standard deviations (*n* = 5).

Based on these optimized separation parameters, a quantitative CE calibration curve was constructed by plotting the integrated peak area against OPA standard concentrations ranging from 0.025% to 0.55% (*w*/*v*). As plotted in Figure 6B, the analytical results demonstrated linear proportionality across the entire tested concentration window. The linear regression equation was established as y = 488.95x − 4.8592, with a correlation coefficient (R^2) of 0.9976. Furthermore, the limit of detection (LOD) was determined to be 0.025% (*w*/*v*) OPA at a signal-to-noise (S/N) ratio greater than 10, with an acceptable precision (CV < 7%, *n* = 5). This linearity and analytical performance confirm that the CE protocol serves as an accurate quantitative benchmark. Consequently, it provides a foundation for the subsequent cross-validation and practical performance evaluation of the proposed colorimetric test strips in real-world clinical applications.

3.6. Cross-Validation and Practical Application in Clinical Disinfectants

To demonstrate the practical utility and quantitative accuracy of the developed microfluidic colorimetric sensor, cross-validation was performed against the established capillary electrophoresis (CE) reference method. Initially, the comparison was conducted

using idealized OPA standard solutions (0.24–0.40%, *w*/*v*) prepared in the standardized 35 mM PB (pH 7.4) matrix. As illustrated in the correlation plot (Figure 7A), the concentrations determined by the proposed test strips exhibited quantitative agreement with those obtained by the CE method. The linear regression equation, y = 0.962x + 0.0127, accompanied by a correlation coefficient (R^2 = 0.9859), indicates the absence of significant proportional errors (slope ≈ 1) and constant bias (intercept ≈ 0) under controlled matrix conditions. Furthermore, precision analysis yielded a coefficient of variation (CV) ranging from 0.8% to 3.3%, satisfying the requirements for reliable quantitative analysis.

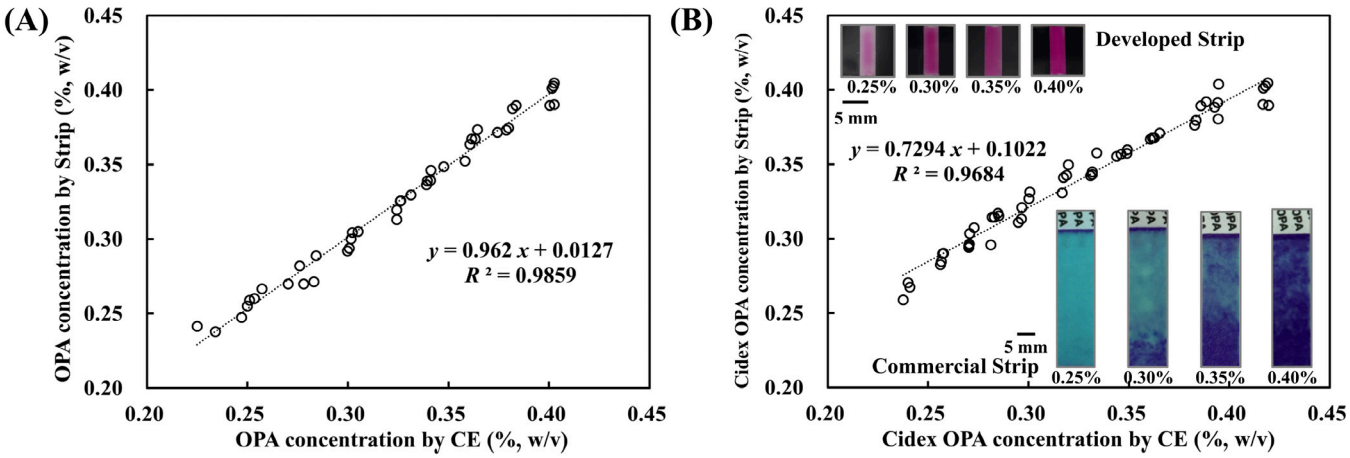

Figure 7. Cross-validation between the developed sensor and the CE reference method. Correlation plots of OPA concentrations (0.24–0.40%, *w*/*v*) for (**A**) idealized standards in 35 mM PB and (**B**) commercial CIDEX OPA solutions diluted with deionized water. Insets in (**B**) visually compare the colorimetric responses of the developed strips (**top**) and commercial CIDEX strips (**bottom**) at specific CIDEX OPA concentrations (0.25%, 0.30%, 0.35%, and 0.40%). Dotted lines represent linear regression fits. Each open circle represents a single independent measurement.

Subsequently, the analytical evaluation was extended to real-world clinical samples using the commercial CIDEX OPA solution. To accurately simulate the physical dilution caused by residual rinse water inside pre-cleaned endoscopes, the CIDEX stock was directly diluted with deionized (DI) water to the critical monitoring range of 0.24–0.40% (*w*/*v*). This preparation strategy aligns with the "negative control" validation concept outlined in the manufacturer's Instructions for Use (IFU) for commercial strips [23]. The IFU mandates a deliberate failure test (e.g., a 50% dilution with deionized water) to simulate a sub-MEC condition. By adopting and expanding upon this standard practice, we evaluated the sensors' reliability across the critical decision-making window. As shown in Figure 7B, the correlation between the proposed test strips and the CE method for these real samples yielded the regression equation y = 0.7294x + 0.1022 (R^2 = 0.9684). As observed from the correlation profile, the slope deviation (approximately 0.73) is primarily driven by a systematic overestimation at lower OPA concentrations. This phenomenon is a direct consequence of the physical dilution of the intrinsic sample matrix. The fresh CIDEX stock contains approximately 43–44 mM PB. When heavily diluted with DI water to reach lower OPA levels, the intrinsic buffering capacity is proportionally diminished. For instance, at a 0.30% CIDEX OPA concentration, the sample solution only retains roughly 23–24 mM PB. Compared to the standardized 35 mM PB used for establishing the calibration curve, this weakened buffering capacity is more easily overcome by the OPA-induced NaOH (Equation (1)), leading to an amplified pH elevation and a consequently overestimated optical readout.

This dilution approach accurately simulates the worst-case boundary conditions encountered during actual endoscope reprocessing, where cumulative residual rinse water

progressively dilutes the disinfectant down to the critical MEC. At the targeted 0.30% MEC threshold, the optical readout is only slightly overestimated by approximately 0.02% (i.e., a true 0.30% CIDEX OPA sample consistently registers as 0.32% on the sensor). Based on this investigation, the diagnostic threshold programmed into the automated sensing platform was strategically adjusted. By setting the warning trigger to 0.32% OPA, the system accurately displays a "[FAIL]" alert, promptly directing the operator to replace the disinfectant. Furthermore, it should be noted that routine endoscope reprocessing and OPA monitoring are strictly performed in controlled indoor clinical environments (typically air-conditioned at 20–28 °C). Because the sensor was calibrated and operated under these stable ambient conditions, temperature-induced variations in the reaction kinetics are negligible for its intended application.

Beyond digital quantification, the proposed microfluidic platform provides distinct visual advantages compared with commercial products. As depicted in the inset photographs of Figure 7B, the commercial ASP CIDEX™ OPA Solution Test Strips exhibit macroscopic color heterogeneity. Although their package insert claims the capability to reliably verify the 0.30% MEC threshold, practical evaluations reveal limitations. Slight color patchiness begins to emerge even at a higher concentration of 0.40%, and patchy discoloration becomes evident at 0.35%. Their varying blue-to-purple color development is affected by uneven reagent distribution and intrinsic chromatographic wicking effects inherent to conventional porous paper substrates. This macroscopic non-uniformity makes subjective visual interpretation by operators ambiguous and susceptible to critical misdiagnoses, particularly when differentiating concentrations near the MEC threshold. Furthermore, the manufacturer's instructions mandate that the results must be visually read at exactly 90 s. This strict temporal constraint imposes considerable operational difficulties and introduces human timing errors during busy clinical workflows.

In contrast, the developed test strips demonstrate a homogeneous colorimetric progression. This spatial uniformity is attributed to the enclosed 5.4 μL microfluidic self-metering design and the engineered micro-cavities (as discussed in Section 3.2), which eliminate operator-induced volumetric errors and edge pooling. Paired with the automated steady-state readout algorithm, the proposed sensing platform provides an unambiguous, objective, and accurate "[PASS]" or "[FAIL]" diagnostic result without the constraint of strict manual timing, overcoming the critical limitations of traditional commercial counterparts.

4. Conclusions

This study developed a portable multi-spectral colorimetric sensing platform and structurally engineered microfluidic test strips for reliable quantitative monitoring of *ortho*-phthalaldehyde (OPA) disinfectants. By integrating a confined microfluidic geometry and cross-hatched micro-structures, the test strips achieved precise capillary-driven volumetric self-metering (5.4 μL) and eliminated edge pooling, ensuring uniform color development.

Analytically, the system integrates a matrix-matched reagent formulation, an interference-free indicator, and an automated steady-state ratiometric readout algorithm to effectively counteract physical dilution and spectral interference. This integration overcomes the subjective visual ambiguity and operator-dependent timing errors inherent in traditional testing workflows.

Cross-validation against a capillary electrophoresis (CE) reference benchmark confirmed quantitative accuracy (R^2 = 0.9684) even under physical dilution of real-world CIDEX OPA solutions. This robust correlation enabled the establishment of a matrix-compensated 0.32% diagnostic threshold for unambiguous and automated "[PASS]" or "[FAIL]" alerts. Consequently, the developed platform provides a fully objective, point-of-care diagnostic solution. Furthermore, compared to our previously developed electrochem-

ical and fluorescent flow injection methods that require complex electrode modifications or continuous liquid handling, this microfluidic dry chemistry architecture eliminates the need for external reagent preparation, achieving true point-of-care readiness and significant cost-effectiveness.

Beyond OPA monitoring, the engineered plastic strips possess significant translational value for industrial mass production. The cross-hatched micro-structures can be readily scaled using continuous ultrasonic embossing. Coupled with mature polymer lamination and coating techniques, the unit material cost is highly competitive, estimated at mere cents per test. Ultimately, this microfluidic architecture demonstrates significant translational potential as a universal platform for broad point-of-care applications across various dry chemistry optical detection fields.

Author Contributions: Conceptualization, H.-Y.H. and T.-J.C.; methodology, H.-Y.H.; software, H.-Y.C.; validation, H.-Y.H.; formal analysis, H.-Y.H.; investigation, H.-Y.H. and H.-Y.C.; resources, T.-J.C. and R.L.C.C.; writing—original draft preparation, H.-Y.H.; writing—review and editing, H.-Y.H., R.L.C.C., H.-Y.C. and T.-J.C.; visualization, H.-Y.H. and H.-Y.C.; supervision, T.-J.C. and R.L.C.C.; funding acquisition, T.-J.C. and R.L.C.C. All authors have read and agreed to the published version of the manuscript.

Funding: This research received no external funding.

Institutional Review Board Statement: Not applicable.

Informed Consent Statement: Not applicable.

Data Availability Statement: Raw data are available from the corresponding author upon reasonable request.

Acknowledgments: The authors gratefully acknowledge the generous material support that facilitated the fabrication of the sensing strips in this work. Specifically, we extend our appreciation to Nan Ya Plastics Corporation (Kaohsiun, Taiwan) for providing the white PET base films (HY21), Nitto Denko Corporation (Osaka, Japan) and JinChung Material Corporation (New Taipei, Taiwan) for supplying the black double-sided adhesive tape (5615BN), and E-Miracle Composite Co., Ltd. (Tokyo, Japan) for contributing the hydrophilic cover membrane (HA2).

Conflicts of Interest: The authors declare no conflicts of interest.

Abbreviations

The following abbreviations are used in this manuscript:

CE	Capillary electrophoresis
HLD	High-level disinfection
MEC	Minimum effective concentration
NdFeB	Neodymium magnets
OPA	*ortho*-Phthalaldehyde
PB	Phosphate buffer
POC	Point-of-care
PVP	Polyvinylpyrrolidone
µPADs	Paper-based microfluidic analytical devices
ADC	Analog-to-digital converter
PDA	Photodiode array
PET	Polyethylene terephthalate
SDS	Sodium dodecyl sulfate

Appendix A

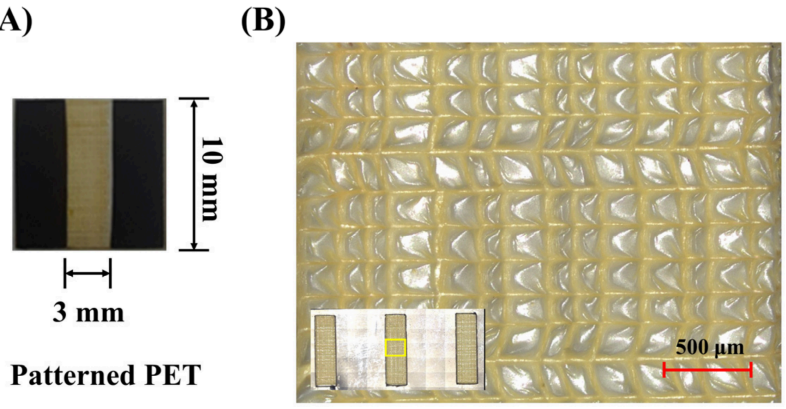

Figure A1. Visual verification of reagent distribution using thymol blue as a colored surrogate. (**A**) Macroscopic photograph showing uniform reagent distribution without edge pooling. (**B**) Optical micrograph revealing the dye sequestered within the cross-hatched micro-grooves. The test strips were fabricated by dispensing 1.8 µL of a 3X concentrated surrogate solution—comprising 6.0 mM thymol blue sodium salt, 60 mM Tris-HCl, 9 mM citric acid, 210 mM Na_2SO_3, 0.09% Tween-20, and 6.0% (*w*/*v*) PVP-360—onto the patterned PET film.

References

1. Günşahin, D.; Şandru, V.; Constantinescu, G.; Ilie, M.; Cabel, T.; Popescu, R.; Ungureanu, B.S.; Miron, V.D.; Balan, G.G.; Cotigă, D.; et al. A Comprehensive Review of Digestive Endoscopy-Associated Infections: Bacterial Pathogens, Host Susceptibility, and the Impact of Viral Hepatitis. *Microorganisms* **2025**, *13*, 2128. [CrossRef] [PubMed]
2. Rutala, W.A.; Boyce, J.M.; Weber, D.J. Disinfection, sterilization and antisepsis: An overview. *Am. J. Infect. Control* **2023**, *51*, A3–A12. [CrossRef] [PubMed]
3. Day, L.W.; Muthusamy, V.R.; Collins, J.; Kushnir, V.M.; Sawhney, M.S.; Thosani, N.C.; Wani, S. Multisociety guideline on reprocessing flexible GI endoscopes and accessories. *Gastrointest. Endosc.* **2021**, *93*, 11–33.e16. [CrossRef] [PubMed]
4. Food and Drug Administration. FDA-Cleared Sterilants and High Level Disinfectants with General Claims for Processing Reusable Medical and Dental Devices. Available online: https://www.fda.gov/medical-devices/reprocessing-reusable-medical-devices-information-manufacturers/fda-cleared-sterilants-and-high-level-disinfectants-general-claims-processing-reusable-medical-and (accessed on 12 May 2026).
5. Ofstead, C.L.; Hopkins, K.M.; Buro, B.L.; Eiland, J.E.; Wetzler, H.P. Challenges in achieving effective high-level disinfection in endoscope reprocessing. *Am. J. Infect. Control* **2020**, *48*, 309–315. [CrossRef] [PubMed]
6. Centers for Disease Control and Prevention. Chemical Disinfectants: Guideline for Disinfection and Sterilization in Healthcare Facilities. Available online: https://www.cdc.gov/infection-control/hcp/disinfection-sterilization/chemical-disinfectants.html (accessed on 12 May 2026).
7. Cooke, R.P.D.; Goddard, S.V.; Whymant-Morris, A.; Sherwood, J.; Chatterly, R. An evaluation of Cidex OPA (0.55% *ortho*-phthalaldehyde) as an alternative to 2% glutaraldehyde for high-level disinfection of endoscopes. *J. Hosp. Infect.* **2003**, *54*, 226–231. [CrossRef] [PubMed]
8. Venkatesh, S.; Kuthandapani, S.; Marudavanan, R. A comparative study of efficacy of disinfectants used for flexible endoscopes: Glutaraldehyde versus *ortho*-phthalaldehyde. *Sch. J. App. Med. Sci.* **2014**, *2*, 1408–1412.
9. Alfa, M.J. Monitoring and improving the effectiveness of cleaning medical and surgical devices. *Am. J. Infect. Control* **2013**, *41*, S56–S59. [CrossRef] [PubMed]
10. Centers for Disease Control and Prevention. Factors Affecting the Efficacy of Disinfection and Sterilization. Available online: https://www.cdc.gov/infection-control/hcp/disinfection-sterilization/efficacy-factors.html (accessed on 12 May 2026).
11. Yamamoto, S.; Hachiya, Y.; Yuasa, E.; Takeuchi, A.; Ishidao, T.; Mihara, M.; Terauchi, Y.; Ichiba, M.; Hori, H. Evaluation of the ceiling levels of *ortho*-phthalaldehyde exposure among health care workers engaged in endoscope disinfection: A new methodology using video-exposure monitoring. *J. Occup. Health* **2020**, *62*, e12139. [CrossRef] [PubMed]
12. Chen, R.L.C.; Hsieh, B.-C.; Lin, J.-S.; Cheng, T.-J. An Electrochemical *o*-Phthalaldehyde Sensor Using a Modified Disposable Screen-Printed Electrode with Polyacrylate Hydrogel for Concentration Verification of Clinical Disinfectant. *Biosensors* **2023**, *13*, 485. [CrossRef] [PubMed]
13. Rutala, W.A.; Weber, D.J. Disinfection and sterilization: An overview. *Am. J. Infect. Control* **2013**, *41*, S2–S5. [CrossRef] [PubMed]

14. Chen, H.-Y.; Chen, R.L.C.; Hsieh, B.-C.; Cheng, T.-J. Determination of *o*-phthalaldehyde for dose verification of the clinical disinfectant by fluorescent sequential injection analysis. *Anal. Sci.* **2023**, *39*, 2007–2017. [CrossRef] [PubMed]
15. Rogers, C.A.; Gaskin, S.E.; Thredgold, L.D.; Pukala, T.L. An approach to quantify *ortho*-phthalaldehyde contamination on work surfaces. *Ann. Work Expo. Health* **2023**, *67*, 886–894. [CrossRef] [PubMed]
16. Vannecke, C.; Baré, S.; Bloomfield, M.; Massart, D.L. An experimental design approach to the optimisation of a flow injection analysis method for glycine. *J. Pharm. Biomed. Anal.* **1999**, *18*, 963–973. [CrossRef] [PubMed]
17. Oh, J.-A.; Shin, H.-S. Determination of *ortho*-phthalaldehyde in water by high performance liquid chromatography and gas chromatography–mass spectrometry after hydrazine derivatization. *J. Chromatogr. A* **2012**, *1247*, 99–103. [CrossRef] [PubMed]
18. Yetisen, A.; Akram, M.; Lowe, C. Paper-based microfluidic point-of-care diagnostic devices. *Lab Chip* **2013**, *13*, 2210–2251. [CrossRef] [PubMed]
19. Cate, D.M.; Adkins, J.A.; Mettakoonpitak, J.; Henry, C.S. Recent Developments in Paper-Based Microfluidic Devices. *Anal. Chem.* **2015**, *87*, 19–41. [CrossRef] [PubMed]
20. Shen, L.; Hagen, J.; Papautsky, I. Point-of-care colorimetric detection with a smartphone. *Lab Chip* **2012**, *12*, 4240–4243. [CrossRef] [PubMed]
21. Rateni, G.; Dario, P.; Cavallo, F. Smartphone-Based Food Diagnostic Technologies: A Review. *Sensors* **2017**, *17*, 1453. [CrossRef] [PubMed]
22. Bui, T.H.; Thangavel, B.; Sharipov, M.; Chen, K.; Shin, J.H. Smartphone-Based Portable Bio-Chemical Sensors: Exploring Recent Advancements. *Chemosensors* **2023**, *11*, 468. [CrossRef]
23. Advanced Sterilization Products. CIDEX™ OPA Solution Test Strips Instructions for Use. 2020. Available online: https://aspsolutions.my.salesforce.com/sfc/p/#5A000000CNKq/a/UU000001RMn9/r19.SJD.xuX5IytPOWp8ta3K55qwbwOAbV_y5Rtmp0I (accessed on 12 May 2026).
24. Hsiao, H.-Y.; Chen, R.L.C.; Chou, C.-C.; Cheng, T.-J. Hand-held Colorimetry Sensor Platform for Determining Salivary α-Amylase Activity and Its Applications for Stress Assessment. *Sensors* **2019**, *19*, 1571. [CrossRef] [PubMed]
25. Xie, N.; Dong, X.; Song, B.; Li, J.; Wang, Z. Simultaneous determination of o-phthalaldehyde, *p*-chloro-*m*-xylenol and triclosan in compound chemical disinfectants and daily chemicals by micellar electrokinetic chromatography. *Chin. J. Chromatogr.* **2013**, *31*, 64–70. [CrossRef] [PubMed]
26. Chen, J.-J.; Lee, Y.-C.; Cheng, T.-J.; Hsiao, H.-Y.; Chen, R.L.C. Determination of glucosamine content in nutraceuticals by capillary electrophoresis using in-capillary OPA labeling techniques. *J. Food Drug Anal.* **2006**, *14*, 203–206. [CrossRef]
27. Zuman, P. Reactions of Orthophthalaldehyde with Nucleophiles. *Chem. Rev.* **2004**, *104*, 3217–3238. [CrossRef] [PubMed]
28. Moitessier, C.; Kital, K.; Danjou, P.-E.; Cazier-Dennin, F. 4-Methoxy-*ortho*-phthalaldehyde: A promising derivatizing agent for the fluorimetric evaluation of histamine in seafood. *Talanta Open* **2020**, *2*, 100014. [CrossRef]
29. Paudel, A.; Nies, E.; Van den Mooter, G. Relating Hydrogen-Bonding Interactions with the Phase Behavior of Naproxen/PVP K 25 Solid Dispersions: Evaluation of Solution-Cast and Quench-Cooled Films. *Mol. Pharm.* **2012**, *9*, 3301–3317. [CrossRef] [PubMed]
30. Pandi, P.; Bulusu, R.; Kommineni, N.; Khan, W.; Singh, M. Amorphous solid dispersions: An update for preparation, characterization, mechanism on bioavailability, stability, regulatory considerations and marketed products. *Int. J. Pharm.* **2020**, *586*, 119560. [CrossRef] [PubMed]
31. Salin, A.A.; Galeev, A.D.; Ponikarov, S.I. Study of the Evaporation of Hydrochloric Acid: Modeling and Experiment. *J. Eng. Phys. Thermophys.* **2014**, *87*, 753–762. [CrossRef]
32. Finšgar, M.; Milošev, I. Inhibition of copper corrosion by 1,2,3-benzotriazole: A review. *Corros. Sci.* **2010**, *52*, 2737–2749. [CrossRef]

Disclaimer/Publisher's Note: The statements, opinions and data contained in all publications are solely those of the individual author(s) and contributor(s) and not of MDPI and/or the editor(s). MDPI and/or the editor(s) disclaim responsibility for any injury to people or property resulting from any ideas, methods, instructions or products referred to in the content.